A Quantum Chemical Study of the Synthesis of Prostaglandin G_2 by the Cyclooxygenase Active Site in Prostaglandin Endoperoxide H Synthase 1

L. Mattias Blomberg,* Margareta R. A. Blomberg, and Per E. M. Siegbahn

Department of Physics, Stockholm Center for Physics, Astronomy and Biotechnology, Stockholm University, SE-106 91 Stockholm, Sweden

Wilfred A. van der Donk

Department of Chemistry, University of Illinois at Urbana-Champaign, 600 S. Mathews Ave., Urbana, Illinois 61801

Ah-Lim Tsai

Department of Internal Medicine, University of Texas Health Science Center at Houston, 6431 Fannin Street, Houston, Texas 77030

Received: October 14, 2002; In Final Form: January 27, 2003

The mechanism for prostaglandin G_2 synthesis in the cyclooxygenase active site of prostaglandin H synthase has been investigated using hybrid density functional theory (B3LYP). The calculations show that the six-step radical mechanism for the transformation of arachidonic acid to prostaglandin G_2 suggested by Hamberg and Samuelsson is energetically feasible. The overall driving force for the reaction starting with the arachidonic acid and the active-site tyrosyl radical is estimated to be about 37 kcal/mol, and two barriers are found to be about 15 kcal/mol, in good agreement with the experimental rate corresponding to a barrier of 14.8 kcal/mol. Competing reactions are also investigated.

I. Introduction

Prostaglandin H synthase (PGHS) is the key regulatory enzyme in prostaglandin biosynthesis. Two PGHS isozymes are known with different physiological roles and expression levels. The constitutive isozyme (PGHS-1) is ascribed housekeeping functions, whereas the inducible isozyme (PGHS-2) is associated with pathological processes[1]. The overall protein folds of the isozymes are very similar, and residues in the catalytic domains are highly conserved.[2−5] Recently, several inhibitors with selectivity for PGHS-2 have been developed as replacements for nonselective nonsteroidal antiinflammatory drugs (NSAIDs) that have attracted much attention because of their successes in suppressing side effects. Similarly, the reaction mechanism of the fascinating conversion of arachidonic acid to prostaglandin H_2 (PGH_2) has been the subject of much interest. PGHS is a single hemoprotein that exhibits two enzyme activities: a cyclooxygenase that catalyzes the dioxygenation of arachidonic acid (AA) to yield prostaglandin G_2 (PGG_2), and a peroxidase that converts PGG_2 to PGH_2 (reaction 1).

Although the active sites are physically distinct, there are many indications of a mechanistic linkage between the peroxidase and cyclooxygenase activities.[6] This linkage is the basis for the remarkable autocatalytic behavior of the cyclooxygenase activity.

The current hypothesis to account for the linkage between PGHS activities (Figure 1) proposes that an oxidized peroxidase intermediate generates the key enzyme oxidant for cyclooxygenase catalysis: reaction of either PGHS isoform with peroxide forms peroxidase compound I (step 1), which oxidizes a tyrosine residue in the protein to form a tyrosyl radical (step 2). Peroxide-induced tyrosyl radicals have been detected in both PGHS-1 and PGHS-2.[7−10] The tyrosyl radical is postulated to abstract a hydrogen atom from C13 of AA to generate a protein-bound arachidonyl radical (step 3), which initiates a cascade of radical

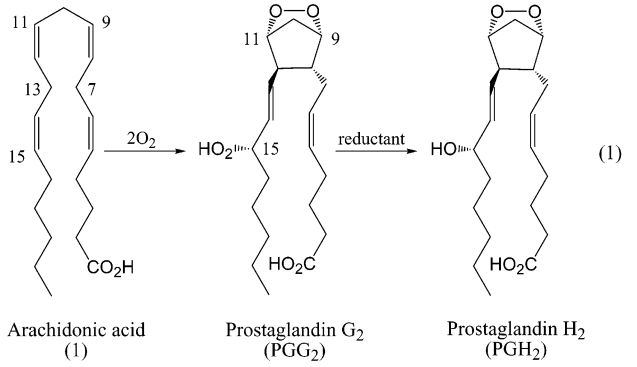

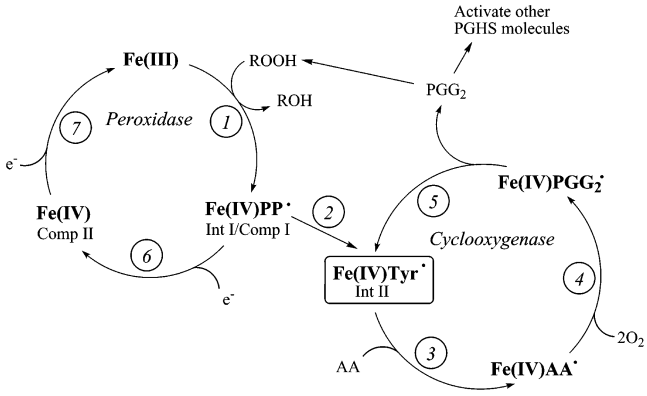

Figure 1. Current PGHS mechanistic model.[8] Both intermediate I and compound II can also be cycled back to the resting state by endogenous or exogenous reducing cosubstrates (steps 6 and 7).

10.1021/jp027204h CCC: $25.00
Published on Web 03/18/2003

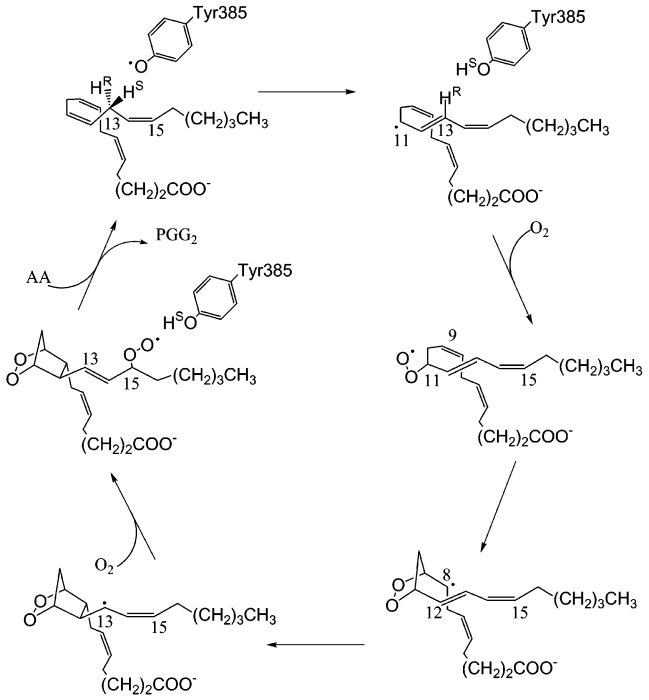

Figure 2. Mechanistic model of the cyclooxygenase reaction.

reactions that incorporate two molecules of O_2 and result in a PGG_2 radical (step 4). The tyrosyl radical is regenerated by abstraction of its phenoxyl hydrogen atom by the PGG_2 radical to produce the final product of the cyclooxygenase reaction, PGG_2 (step 5). A detailed chemical mechanism for the transformation of arachidonic acid to PGG_2 was proposed by Hamberg and Samuelsson,[11] see Figure 2. In this sequence, abstraction of the *proS*-hydrogen atom from C13 of arachidonic acid forms a C11−C15 pentadienyl radical. Reaction of this radical with O_2 gives 11-peroxyl radical and subsequent cyclization to form a 9,11-peroxo bridge and a radical at C8. Cyclization of the radical at C8 onto the diene at C12 generates an allyl radical spanning C13−C15, which attacks a second O_2 molecule to give a hydroperoxyl (PGG_2) radical. The final step is reduction of the PGG_2 radical by the tyrosine in the active site to give PGG_2. Although this scheme provides an elegant explanation of the observed product, none of the proposed intermediates have been identified for 3 decades because of experimental difficulties. Moreover, the regulation of the regio- and stereospecificity by PGHS is not completely solved, although recent crystallographic and mutagenesis studies have provided important insights.[12−15]

The chemical competence of the tyrosyl radicals to generate AA radicals in both isoforms has been established by anaerobic single-turnover studies.[16,17] The AA-derived radical formed in these studies has been characterized by EPR and a series of site-specific-deuterated substrates.[16−19] These studies confirm that the radical in PGHS-2 is a pentadienyl radical, C10 having two and C16 one β-protons interacting strongly with the unpaired electron to facilitate endoperoxide formation between C9 and C11 and ring closure between C8 and C12. Under regular turnover conditions, a primary kinetic isotope effect has been observed using arachidonic acid tritiated at the *proS*-position,[11] and the pentadienyl radical has only been observed under anaerobic conditions. As a result, trapping of subsequent radical intermediates will be challenging and has not been achieved to date. Furthermore, because the observed pentadienyl radical was characterized under nonnative conditions, the caveat exists that it is not the actual intermediate during turnover.[19]

This report describes a theoretical approach to address the feasibility of the mechanism in Figure 2 and provides information regarding the energetics of the individual steps. Moreover, such theoretical calculations can assist in locating additional stabilized radical intermediates and provide information about barriers of rotation and spin density distribution. Reported here are density functional theory (DFT) calculations using the X-ray crystallographic data of AA-bound PGHS-1[5] as starting conformations for the catalytic tyrosyl radical and arachidonic acid.

II. Computational Details

IIa. Methods. The geometries of the stationary points involved in the reaction studied were optimized using Becke's[20] three-parameter hybrid exchange functional combined with the Lee−Yang−Parr[21] correlation functional (B3LYP) with valence double-ζ (d95v) basis sets on all atoms. The intermediates are open-shell systems and are treated using unrestricted B3LYP. All degrees of freedom were optimized, and the stationary points were further characterized by vibrational frequency analysis at the same level of theory. Zero-point and thermal corrections were computed using the unscaled frequencies. The transition states obtained were confirmed to have only one imaginary frequency of the Hessian. The final B3LYP energies were evaluated for the optimized geometries using the 6-311+G-(2d,2p) triple-ζ basis set, which includes one diffuse function on heavy atoms and two polarization functions on both hydrogens and second-row atoms. The dielectric effects from the surrounding environment were obtained for all stationary points (minima and transition states) using the Jaguar self-consistent reaction field method with its Poisson−Boltzmann solver[22] and the 6-311+G(d,p) basis set. The dielectric constant was set equal to 4, which corresponds to a dielectric constant of about 3 for the protein and 80 for the water medium surrounding the protein.[23] The probe radius of the solvent was set to 1.4 Å, which corresponds to a water molecule. The relative energies discussed below are Gibb's free energies with the solvent effects included. Normal errors of the B3LYP method and different aspects of modeling enzyme active sites are described in recent reviews.[24−26]

The two-layered hybrid ONIOM[27−29] method implemented in the Gaussian 98 program[30] was also applied to estimate some of the effects of the surrounding protein. Only the intermediates and no transition states were treated using this method. To avoid chemical artifacts, the cut between the two layers of the ONIOM model is done only in carbon−carbon single covalent bonds. The same model as treated with pure quantum mechanical (QM) method is used as the high-level part of the ONIOM calculations, see further below. The results of the different models should thus be directly comparable. The two-layered ONIOM extrapolated energy[27] is defined as follows:

$$E_{\mathrm{ONIOM2}} = E_3 - E_1 + E_2 \qquad (1)$$

E_3 is the energy of the entire system calculated at the low level of theory, and E_1 and E_2 are the energies of the small model (inner layer) determined at the low and the high level of theory, respectively. The B3LYP hybrid density functional method[20,21] was used as the high-level method, and for the outer layer, the low-level semiempirical Austin model 1 (AM1)[31] was used. For the ONIOM geometry optimizations, the double-ζ valence basis set were used, and the final energy evaluations in the optimized structures were carried out using the 6-311+G(2d,2p) triple-ζ basis set. The B3LYP results on the first hydrogen atom abstraction step were found to diverge from comparable

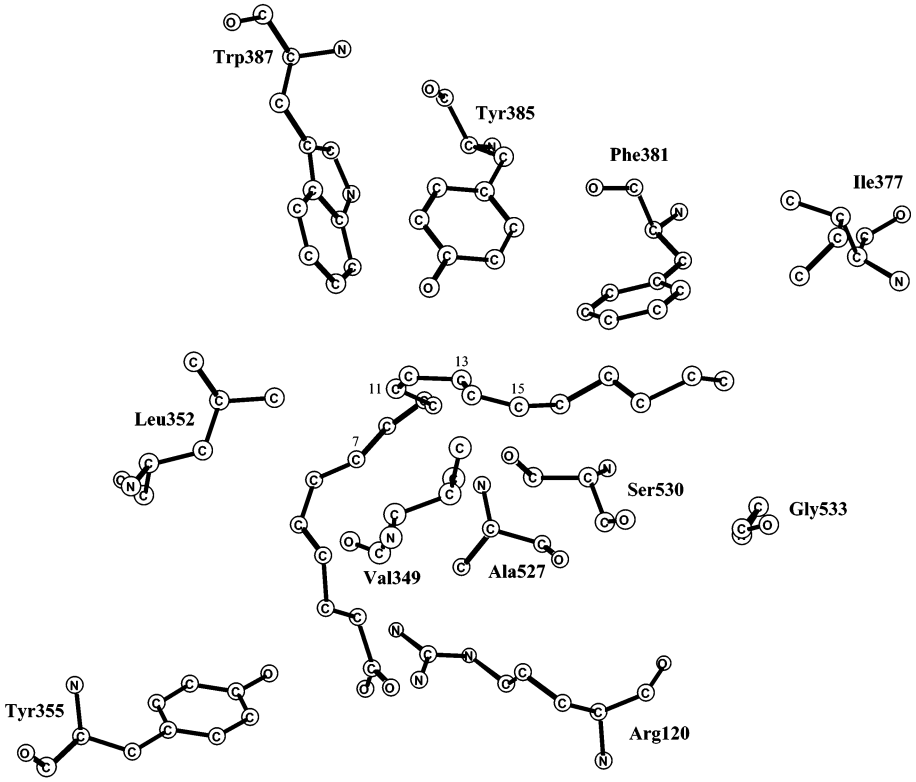

Figure 3. X-ray structure of the active site region of prostaglandin H synthase 1.[5]

experimental results of bond dissociation energies (BDE).[32,33] Therefore, these BDEs were also evaluated using a G2-MP2[34,35] type of extrapolation scheme:

$$\Delta E = \Delta E_{\mathrm{CCSD(T)/6-31G^*}} + \Delta E_{\mathrm{MP2/6-311+G(2df,2p)}} - \Delta E_{\mathrm{MP2/6-31G^*}} \quad (2)$$

The B3LYP/d95v geometries were used for the MP2 and CCSD-(T) calculations. This scheme provides an effective approach for estimating relative CCSD(T)/6-311+G(2df,2p) energies. The zero-point corrections were taken from the unscaled B3LYP/d95v frequencies.

The Gaussian 98 program[30] was used for all calculations in this study except for the solvation effect calculations, which were carried out with the JAGUAR[36] program.

IIb. Models. The first point to be considered in any quantum chemical study of an enzyme mechanism is to make an appropriate choice of model of the active site and the substrate. The crystal structure of PGHS-1 with arachidonate (AA) bound in the active-site pocket[5] was used as a starting point in this study, see Figure 2. Although there are structural differences between PGHS-1 and PGHS-2,[2−5] the models used will not involve those and the structural differences between the two iso-enzymes are rather small. This means that the results should also be valid for PGHS-2. In PGHS, the substrate AA is a 20 carbon, 4-fold unsaturated acid ((*Z*,*Z*,*Z*,*Z*)-5,8,11,14-eicosatetraenoic acid) in an active site composed of ∼20 amino acids. This system is too large to be treated with DFT methods. Two models were used in the study, one smaller model (model 1) to be treated with the B3LYP functional to examine the suggested mechanism and one larger model (model 2) treated with a two-layered ONIOM model, which incorporates some parts of the surroundings (Figure 4). No water molecules are present in the active site of the crystal structure of PGHS-1[5] used in the present study. The conventional numbering of the carbons in AA is kept throughout this article, see Figure 2.

Model 1 consists of the C7−C16 part of the AA substrate, which is where the radical chemistry is believed to occur. The carboxylate and ω-end of AA have no chemical properties affecting the radical reactions taking place on C8−C15 but introduce pure steric effects when incorporated in the active site of PGHS. In model 1, (*Z*,*Z*,*Z*)-2,5,8-decatriene, no steric effects were taken into account, that is, all degrees of freedom were optimized. The tyrosyl radical is modeled as a phenoxyl radical, and it is only incorporated in the calculations when it takes part in the reaction, that is, in the first and the last reaction steps. Because all species in the system are uncharged and no hydrogen bonds occur, the interaction between the intermediates and the phenol should be small and not vary much between the different stationary points. Thus exclusion of the phenol is not expected to significantly affect the relative energies. The active-site pocket surrounding this part of AA consists of amino acids only giving rise to hydrophobic interactions, see Figure 3, and therefore, the interactions between AA and the surrounding environment are not expected to differ very much through the reaction steps either. Because the polarity of the amino acids surrounding the active site is quite uniform, see Figure 3, these interactions should be rather well described by the polarizable continuum model, which is used together with model 1.

In model 2, the full substrate and the amino acids Tyr385, Tyr355, and Arg120 are incorporated, and in Figure 4, it is indicated which parts of the model were treated at the B3LYP level and which parts were treated at the AM1 level. The distances between the β-carbons of Tyr385, Tyr355, Arg120, and the ω-end (C20) of the substrate were frozen relative to each other with the coordinates taken from the crystal structure,[5] see Figure 4. The freezing is done to keep the shape of the substrate in the active site of PGHS. Arg120 and Tyr355 are incorporated in the model because they position the carboxylate end of AA through a salt bridge and a hydrogen bond, respectively. Arg120 has been shown to be crucial for binding

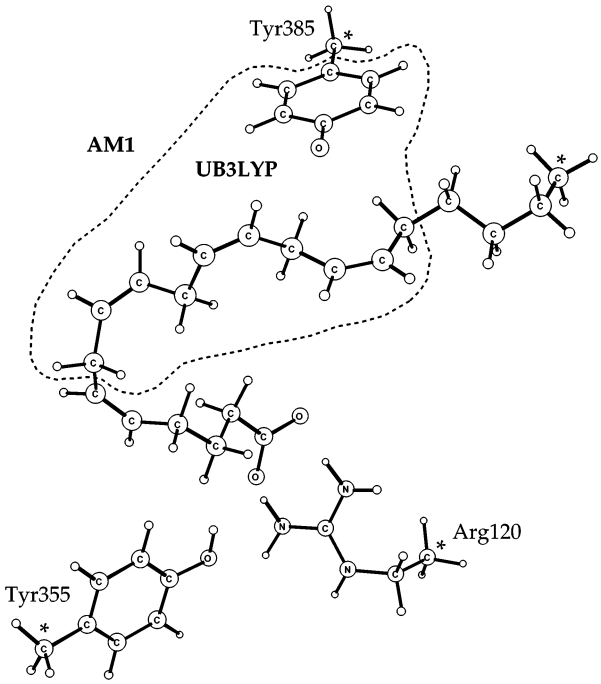

Figure 4. The two layers in the ONIOM model. The restricted carbons in the model are marked with an asterisk.

AA in a reactive conformation in PGHS-1.[37] Recent mutational studies have shown that the residues Ser530 and Val349 control the stereochemistry of the product at C15 in both PGHS-1 and PGHS-2.[12] In the present study, these amino acids are excluded to keep a feasible size of the system in the calculations and because they only have hydrophobic interactions with the substrate. The excluded amino acids will have some steric effects, which may be important for the stereochemistry in the production of PGG_2 and which are thus not fully described in the present model. Even though the relative distances of the three β-carbons and the ω-end are frozen relative to each other, the amino acids have a rather high freedom to move because the adjacent amino acids are not included in the model. Hence, there is no steric hindrance for Tyr385, Arg120, Tyr355, and the substrate, which should enhance their flexibility compared to the enzyme. Therefore, Tyr385 will be able to reach the peroxyl radical on C15 in the last step of the reaction sequence although C20 in AA is frozen and cannot be pulled into the active-site pocket by the cyclizations as it is proposed to do in the enzymatic reaction.[5]

III. Results and Discussion

In this study, the reaction mechanism for PGG_2 formation in the PGHS enzymes proposed by Hamberg and Samuelsson[11] and shown in Figure 2 was investigated. The peroxidase active site of the enzyme becomes oxidized when it reduces peroxides, and it then oxidizes Tyr385 in the cyclooxygenase active site to a tyrosyl radical (Figure 1). Loss of the tyrosine proton is a necessity for the oxidation to occur, but the fate of the proton is still not understood. In this study, the tyrosyl radical is taken as the starting point. The achiral AA is transformed to PGG_2 containing five chiral centers through a radical mechanism and by the addition of 2 equiv of molecular oxygen. The calculated free energies of model 1 for the reaction mechanism in Figure 2 are presented in section IIIa. In section IIIb, the energetics of the intermediates in model 1 (UB3LYP) and model 2 (ONIOM) are compared to investigate the effects of some of the surroundings and of increasing the size of the substrate model. In section IIIc, corrections to the calculated energies are introduced using experimental results for similar reactions. In section IIId, the calculated energetics of reactions competing with the production of PGG_2 are presented and the selectivities of certain steps are discussed.

TABLE 1: Calculated Reaction Energies and Barrier Heights (in kcal/mol) of Each Step in the Production of PGG_2[a]

	UB3LYP/ 6-311+ G(2d,2p)	ΔZPE[b]	$\Delta(H(T))$[b,c]	$-T\Delta S$[b]	ΔG_g^0	$\Delta\Delta G_{solv}$[d]	ΔG_{sol}^0
TS1	10.0	−2.8	−0.8	4.0	10.4	1.9	12.3
step 1	−17.4	0.1	−0.1	2.0	−15.4	1.9	−13.5
TS2	1.6	1.3	−0.6	10.7	13.0	−1.9	11.1
step 2	−10.5	3.5	−0.7	11.0	3.3	−2.5	0.8
TS3	12.4	−0.6	−0.7	2.3	13.4	−1.5	11.9
step 3	5.0	−0.1	−0.4	1.1	5.6	−0.7	4.9
TS4	7.7	−0.3	−1.0	3.5	9.9	0.1	10.0
step 4	−17.8	1.9	−1.1	3.7	−13.3	−0.3	−13.6
step 5	−17.8	3.4	−0.8	11.3	−3.9	−3.1	−7.0
TS6	12.4	−3.4	−0.6	2.7	11.1	−0.6	10.5
step 6	1.5	−0.6	−0.1	1.1	1.9	−2.1	−0.2

[a] Contributions to the relative energies from different effects are also given. [b] UB3LYP/d95v frequencies, see the section on computational details. [c] Thermal correction to the enthalpy. [d] UB3LYP/6-311+G(d,p), see the section on computational details.

IIIa. Calculated Energetics for the Synthesis of PGG_2. In this section, each individual step in the reaction mechanism proposed by Hamberg et al. is discussed, and the resulting structures and energies obtained using model 1 are given. The different contributions to the energetics of each step are summarized in Table 1, and the resulting free energy curve is presented in Figure 5.

Abstraction of the proS-Hydrogen of Arachidonic Acid. In the first reaction, the 13*proS*-hydrogen is abstracted by the tyrosyl radical and the pentadienyl radical of AA is formed.[38] In the crystal structure,[5] the substrate is orientated with C13 close to the oxygen on Tyr385 appropriate for the hydrogen abstraction. In the optimized reactant complex, the 13*proS*-hydrogen is pointing toward the phenoxyl radical oxygen and at a distance of 2.5 Å. In the transition state, the spin that is initially distributed over the phenoxyl radical ring is partly transferred to the substrate. The bond between C13 and the 13*proS*-hydrogen is stretched to 1.25 Å, while the distance from the hydrogen to the oxygen of the phenoxyl radical is reduced to 1.37 Å (Figure 6). In the product, all of the spin is transferred to the pentadienyl radical, which is planar and has a high and almost uniform spin population on C11, C13, and C15 (0.48, 0.52, and 0.50, respectively). The spin populations of the substrate are not significantly sensitive to the size of the model.

The calculated barrier for the hydrogen abstraction is 12.3 kcal/mol. Hamberg et al. observed a tritium isotope effect for the 13*proS*-hydrogen abstraction.[11] When transition state theory and the harmonic approximation are used, the kinetic isotope effects (KIE) can be estimated from the B3LYP calculated barriers, yielding $k_H/k_T = 10.8$ for tritium.

Dioxygen Attack on the Pentadienyl Radical. In the second step, dioxygen is believed to approach from the lipid bilayer through a channel ending at the COX active site of PGHS-1. Close to C11 of AA, there is a small pocket to which dioxygen has been proposed to migrate.[5] C11 of the pentadienyl radical would then be in a good position for the attack by dioxygen from the opposite side with respect to the 13*proS*-hydrogen, giving the 11*R*-peroxyl radical intermediate.[39]

In this study, the oxygen was placed opposite to the side of the hydrogen abstraction. A reactant complex minimum was

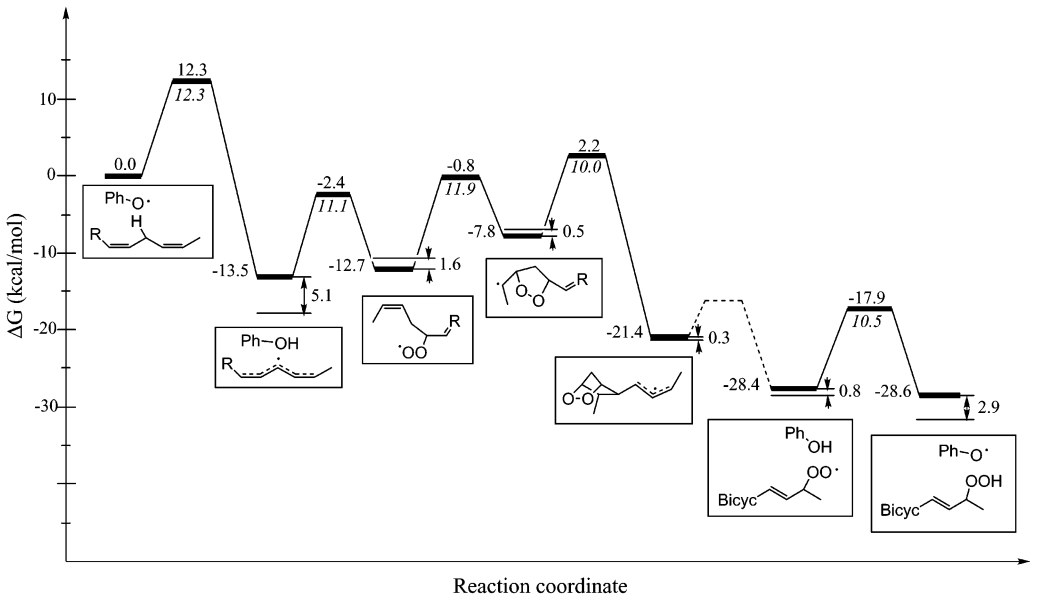

Figure 5. Calculated free-energy surface for the synthesis of PGG_2. The deviations between the ONIOM model (model 2) and the pure DFT model (model 1) are shown in the figure as thin horizontal lines and vertical arrows.

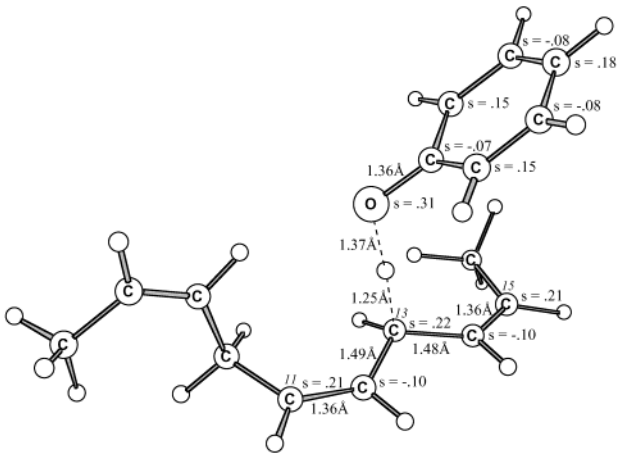

Figure 6. Optimized transition state for reaction step 1 of Figure 2, the abstraction of the *proS*-hydrogen.

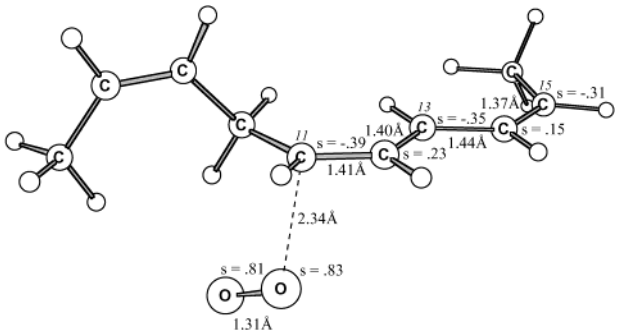

Figure 7. Optimized transition state for reaction step 2 of Figure 2, the attack of O_2 on C11 of the pentadienyl radical.

found, structurally very similar to the ensuing transition state for the C−O bond formation, which indicates a low enthalpy barrier for the reaction. Indeed, the enthalpy barrier of the reaction is only 1.6 kcal/mol relative to the pentadienyl radical and free O_2. Adding entropy (10.7 kcal/mol) and solvation effects raises the barrier to 11.1 kcal/mol. In the transition state, the spin decreases on both O_2 and the pentadienyl radical. The O−O bond distance increases from 1.26 to 1.31 Å as the biradical dioxygen obtains more single-bond character when the peroxyl radical starts to form. In the pentadienyl radical, the C12−C13 and C14−C15 bonds shorten as the localized double bonds start to form (Figure 7). In the product, all of the spin is situated on the two oxygens of the peroxyl radical with a spin population of 0.7 on the primary and 0.3 on the secondary oxygen. The O−O bond distance is 1.38 Å, between the length of a peroxide and a dioxygen bond. The reaction is endergonic by 0.8 kcal/mol.

The calculations above assume that the attack of oxygen is on C11. Because the pentadienyl radical is delocalized over five carbons, O_2 could in principle react with C11, C13, or C15, which is further discussed in section IIId. A second aspect of the O_2 attack is the enantioselectivity. Separation of the products generated by native PGHS-1 shows that as much as 95% of the product is PGG_2.[39] To form PGG_2, both O_2 attacks have to occur from the side opposite to the *proS*-hydrogen abstraction. One explanation for the preference for O_2 attack from this side, as mentioned above, involves dioxygen binding to a pocket beneath C11.[5] The models used in this study are not large enough to incorporate the binding site for oxygen, and the enantioselectivity was therefore not investigated.

Endoperoxide Ring Formation. In the third reaction step, the peroxyl radical must approach C9 to attack the double bond and form the five-membered peroxide ring. This can be achieved by a rotation around the C10−C11 bond. The crystal structure of PGHS-1 with AA in the active site[5] shows that AA is in a conformation with a different C9−C10−C11−C12 dihedral angle (−158°) than the optimized structure of the peroxyl radical (−72°). The C9−C10−C11−C12 dihedral angle of AA in the enzyme implies that the active-site pocket holds the substrate in a conformation with C9 much closer to the formed peroxyl radical and a much smaller rotation around the C10−C11 bond is needed for the reaction to occur. In the optimized transition state, the C9−C10−C11−C12 dihedral angle is 158°, that is, 44° from the value in the crystal structure. The rotation around the C10−C11 bond (130°) in the optimized structure in the calculations necessary for the peroxyl radical attack on the sp^2-carbon should not cost much energy.

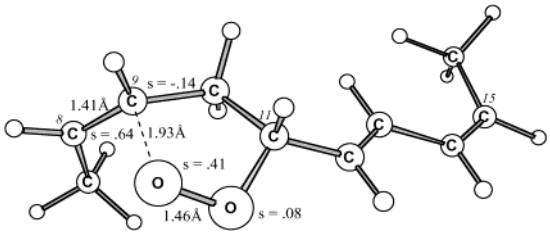

Figure 8. Optimized transition state for reaction step 3 of Figure 2, peroxide cyclization.

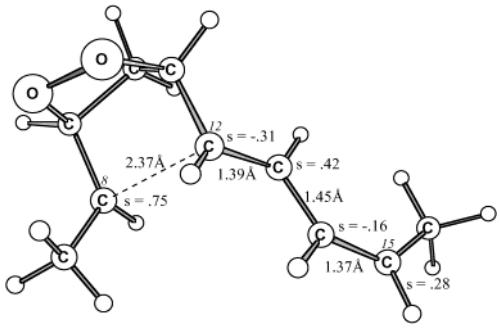

Figure 9. Optimized transition state for reaction step 4 of Figure 2, cyclopentane ring formation.

In the transition state, spin from the peroxyl radical is transferred to the double bond. The distance between the peroxyl oxygen and C9 is 1.9 Å, see Figure 8. The O−O bond length is stretched to 1.46 Å, now almost corresponding to a single bond, and the C═C double bond length is increased to 1.41 Å, which is between the length of a single and double C═C bond.

In the product, all of the spin is localized on C8. The reaction is endergonic by 4.9 kcal/mol, which is reasonable because the peroxide ring contains some strain, approximately 6 kcal/mol,[40] and a thermodynamically less-stable carbon-centered radical is formed. The barrier for the reaction is 11.9 kcal/mol.

Formation of the Cyclopentane Ring. The formation of the bicyclic system in reaction 4 also needs nuclear motion of the reactant to bring C8 close enough to C12 for the reaction to occur. The active-site pocket must also hold the carboxylate end of the substrate in such a way that the correct enantiomer is formed from the sp^2-hybridized radical on C8. C8 and C12 are brought together by rotation around the C10−C11 bond.[5] In the optimized structures, a rotation around C10−C11 of 80° is needed to go from the structure of the C8-radical to the transition state. To obtain the correct stereochemistry on C8 from the optimized peroxide ring, a rotation around the C8−C9 bond of 102° is needed to form the transition state. In the transition state, spin from C8 is transferred and delocalized over C13−C15. The distance between the C8-radical and C12 is 2.37 Å (Figure 9). The double bond of C12−C13 starts to stretch and is 1.39 Å in the transition state. The barrier for the reaction is 10.0 kcal/mol (Figure 5). The reaction is exergonic by 13.6 kcal/mol, which is plausible because a C−C bond is formed and instead of the localized radical on C8 a delocalized allyl radical on C13−C15 is generated.

Dioxygen Attack on the Allyl Radical. In the fifth reaction step, a second molecule of dioxygen attacks C15 of the allyl radical and a peroxyl radical is formed. The O_2 molecule is believed to be situated in the same pocket as that in the reaction between O_2 and the pentadienyl radical described above.[5] Because of the ring system formed in the previous steps, the ω-end of the substrate is pulled into the pocket and C15 will be well positioned above the dioxygen pocket.[5] No transition state has been found for this reaction step because the reaction progresses without a barrier in the calculations. This is plausible bearing in mind the extremely low enthalpy barrier in the O_2 attack on the pentadienyl radical. The entropy effect raises the energy of the product by 13.9 kcal/mol, and forming the transition state should give approximately the same loss in entropy. Hence, a pure entropy barrier is expected but probably less than 7 kcal/mol (this number corresponds to a pure entropy barrier taken from reaction step 2 with zero-point, thermal, and solvation effects added). The height of the barrier is also discussed below in the section on corrections to the energetics. In the product, all spin is located on the two oxygens with a spin population of 0.7 on the primary and 0.3 on the secondary oxygen of the peroxyl radical. The reaction is exergonic by 7.0 kcal/mol.

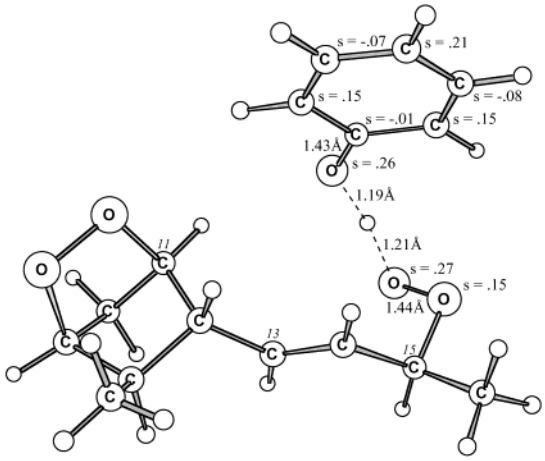

Figure 10. Optimized transition state for reaction step 6 of Figure 2, peroxyl radical abstraction of the phenol hydrogen.

Hydrogen Abstraction by the Peroxyl Radical and Regeneration of the Tyrosyl Radical. In the last reaction, the tyrosyl hydroxyl hydrogen is abstracted by the peroxyl radical forming PGG_2 and a tyrosyl radical. In the transition state, spin is transferred to the tyrosyl hydroxyl oxygen and the aromatic ring (Figure 10). The O−H bond length in tyrosine is stretched to 1.19 Å, and the peroxyl−hydrogen bond distance is decreased to 1.21 Å. The O−O bond distance in the peroxyl radical has increased to 1.44 Å, going from something between a single and a double bond to more single-bond character. In the product, the tyrosyl radical is recovered and the catalytic cycle can be repeated for a new substrate molecule. All of the spin has now been transferred to the tyrosyl radical. This reaction step is thermoneutral (exergonic by 0.2 kcal/mol), and the barrier is 10.5 kcal/mol. The energetics of the entire reaction sequence are shown in Figure 5.

IIIb. ONIOM Model. Two-layered ONIOM calculations were performed on all intermediates of the production of prostaglandin G_2 to study the effect of incorporating more of the active-site pocket, the full substrate, and some structural restrictions. No transition states have been optimized with this model (model 2). In Figure 4, the parts of the enzyme included in the two layers are shown. The restrictions made in model 2 are described in the Computational Details section. Comparison of the relative energies of the two models is presented in the free-energy surface in Figure 5. The energies in Figure 5 using model 1 are Gibbs free energies, while the relative energies between models 1 and 2 are not corrected for entropy or zero-point effects. The maximum deviation between the models is 5.1 kcal/mol. Even though there are some energy deviations between the models, they are not changing the overall view of

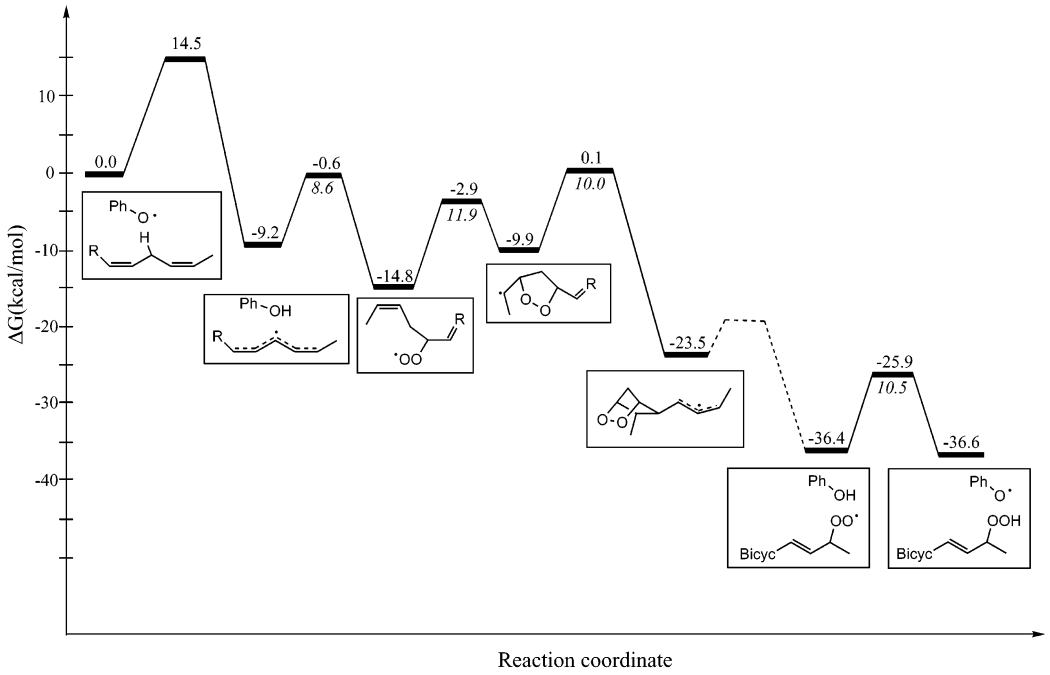

Figure 11. The calculated free-energy surface corrected according to the experimental results described above.

the mechanism. The significance of the size of the deviations in each point should not be over-interpreted. One conclusion drawn from the ONIOM calculations is that the energies are not very sensitive to small structural changes induced by surrounding amino acids. Even though C20 is frozen, there are only small deviations in the energies relative to model 1. The small energy changes due to restrictions in model 2 support the assumption that steric interactions between the enzyme and AA will not change the energetics of the proposed mechanism very much. The free-energy surface for the synthesis of PGG_2 evaluated with model 1 should therefore be reasonably valid for the enzymatic reaction even though the constraints introduced on the substrate by the amino acids in the native active-site pocket are neglected, that is, all degrees of freedom have been optimized.

IIIc. Corrections to the Energetics. In this section, the computational results for individual steps are compared to the energetics of similar gas-phase reactions studied experimentally, where such information is available, and the deviations are used to correct the calculated values. The corrections are made according to the enthalpies of the experimental reactions, and therefore, the energies discussed in this section are gas-phase enthalpies and not free energies with dielectric effects as used in the rest of the paper. An exception is the solvation of molecular oxygen, which is corrected to the free energy of solvation. The individual corrections are discussed below, and the corrected energies are used to construct a new free-energy surface, which is shown in Figure 11 and discussed at the end of this section. The results from G2-MP2 calculations are reported in some cases for comparison (see section II).

Abstraction of the proS-Hydrogen of Arachidonic Acid. No experimental bond dissociation energy (BDE) could be found for (*Z*,*Z*,*Z*)-2,5,8-decatriene, which is used to model AA in the calculations. Instead a comparison was made for the smaller 1,4-pentadiene, which gives a similar pentadienyl radical when the hydrogen atom is abstracted. The exothermicity for the hydrogen abstraction from C3 in 1,4-pentadiene by the phenol radical is 10.6 kcal/mol as calculated from the experimental BDEs,[32,33] while the B3LYP calculations give an exothermicity of 14.9 kcal/mol for the same compound, thus an error of 4.3 kcal/mol. The corresponding value for the abstraction from C13 of the decatriene model is 16.6 kcal/mol, showing that the end substituents are stabilizing the pentadienyl radical by 1.7 kcal/mol. This trend was confirmed in G2-MP2 calculations, giving 2.8 kcal/mol stabilization of the pentadienyl radical of decatriene by the end substituents. The calculated (both B3LYP and G2-MP2) and experimental gas-phase BDEs for 1,4-pentadiene and phenol are given in Table 2. From the table, it can be seen that B3LYP underestimates both binding energies, while G2-MP2 overestimates them. For the phenol, the two methods give a rather similar size of the error, 2.5−3.0 kcal/mol, while for the pentadienyl radical, G2-MP2 has essentially no error (0.4 kcal/mol) and B3LYP has an unusually large error of 6.8 kcal/mol.

TABLE 2: Calculated and Experimental Gas-Phase Values of Bond Dissociation Energies (kcal/mol) for 1,4-Pentadiene and Phenol

	UB3LYP[a]	G2-MP2[a]	exptl value
1,4-pentadiene	69.6	76.8	76.4[b]
phenol	84.5	90.0	87.0[c]
ΔH	−14.9	−13.2	−10.6

[a] For information about the methods, see the section on computational details. [b] Reference 32. [c] Reference 33.

Using the B3LYP error determined for the 1,4-pentadiene, a correction is applied to the computed free energy of the first hydrogen abstraction step, decreasing the exergonicity of the reaction by 4.3 kcal/mol. Because it is likely that also the energy in the transition state region is affected by this error, half of the correction is applied to the transition state, raising the barrier by 2.2 kcal/mol.

O_2-Binding Reactions. The Gibbs free energies for the barriers and products in the reactions of O_2 with the carbon-based radicals are raised significantly because of a large loss in entropy. The major entropy effect originates from using dioxygen in the gas phase as the reactant. Because O_2 in the enzyme is not as free as O_2 in the gas phase, the entropy effect is exaggerated. Hence, the calculated values for the reactions containing O_2-binding have been corrected with the experimental

TABLE 3: Calculated and Experimental Values of the Reaction Enthalpy and the Free-Energy Barrier (kcal/mol) of the Gas-Phase Reaction between O_2 and the Pentadienyl Radical

	calcd model 1	calcd 1,4-pentadiene	exptl[a] 1,4-pentadiene
ΔH^0_{298}	−7.7	−8.1	−12 ± 1
$\Delta G^{\ddagger}_{298}$	13.0	10.9	10.5[b]

[a] Reference 47. [b] Calculated for the reverse reaction, ref 47.

Gibb's free energy for solvation of molecular oxygen. Henry's constant for oxygen in different solvents such as *n*-alkanes, methanol, ethers, and benzene[41−45] has been determined and can be used to calculate the solvation energy for molecular oxygen. The solvation free energies range from 2.2 to 2.8 kcal/mol for the different organic solvents. A mean value of 2.5 kcal/mol has been used as a correction to the computed values for binding of molecular oxygen, lowering the transition state and product energies relative to the reactants.

When dioxygen is covalently linked to the substrate, there is a change in the electronic configuration of the oxygens toward more loosely bound electrons increasing the polarizability. This results in increased van der Waals interactions with the surroundings, which cannot be treated with DFT. Wirstam et al.[46] used molecular mechanics parametrized to estimate van der Waals interactions to evaluate this effect. Increased van der Waals interactions were found to stabilize the O_2-bound product relative to free molecular oxygen. These interactions cancel a part of the entropy effect in O_2-binding. In this study, increased van der Waals interactions in the product of O_2-binding could lower both the transition state and the product. This effect is not included here, but it could make the reaction steps involving molecular oxygen more exergonic and faster.

Dioxygen Attack on the Pentadienyl Radical. The reaction between O_2 and the pentadienyl radical in 1,4-pentadiene has been studied experimentally by a combination of pulsed laser flash photolysis and photoionization mass spectrometry.[47] The reaction enthalpy and the rate of the reaction were determined, see Table 3, in which the calculated values are also given for 1,4-pentadiene, as well as for the decatriene used in the study (model 1). Comparing the calculated reaction enthalpy for 1,4-pentadiene with the experimental one shows that the C−O bond strength is underestimated by 3.9 kcal/mol in the calculations. Therefore an enthalpy correction, stabilizing the product relative to the reactant by 3.9 kcal/mol, is added to the calculated free energy of the second step of the investigated reaction path. The calculated free energy barrier is, on the other hand, very close to the barrier evaluated from the experimental rate constant for the reverse reaction. No correction is made for the barrier of the reaction.

Dioxygen Attack on the Allyl Radical. The reaction between O_2 and the propenyl radical, corresponding to the second addition of molecular oxygen in the PGG_2 synthesis, has also been studied experimentally.[48] The radicals were formed by laser flash photolysis, and the products were detected with a photoionization mass spectrometer. The reaction enthalpy and the rate of the reaction between O_2 and the allyl radical are reported in Table 4, in which the calculated values are also given for propene, as well as for the decatriene (model 1).

Comparing the calculated reaction enthalpy for propene with the experimental one shows that the C−O bond strength in this case is underestimated by 3.4 kcal/mol in the calculations, a value very similar to the corresponding value for the pentadienyl case (3.9 kcal/mol). An enthalpy correction of 3.4 kcal/mol is therefore introduced for the free energy of the reaction step in which the second O_2 molecule is added to the substrate, stabilizing the product relative to the reactant, and thus further increasing the exergonicity of this quite exergonic step. As described above, no transition state was found for this reaction, indicating that the barrier is entirely entropic.

TABLE 4: Calculated and Experimental Values of the Enthalpy and the Barrier (kcal/mol) of the Gas-Phase Reaction between O_2 and the Allyl Radical

	calcd model 1	calcd propene	exptl[a] propene
ΔH^0_{298}	−15.1	−13.8	−17.2 ± 1[b]
$\Delta G^{\ddagger}_{348}$			7.4[c]

[a] Experimental temperature = 348.4 K.[48] [b] Corrected to 298 K, $\Delta H^0_{348} = -17.4$.[48] [c] Calculated for the reverse reaction, ref 48.

Corrected Free-Energy Surface. The resulting free-energy surface for the proposed reaction mechanism of PGG_2 formation, incorporating the corrections described above to the calculated energies, is shown in Figure 11. The barrier of the first hydrogen abstraction step is raised from 12.3 to 14.5 kcal/mol, and the exergonicity of the reaction is decreased from 13.5 to 9.2 kcal/mol. The corrected exergonicity of the reaction agrees rather well with the experimental value of 7.6 kcal/mol calculated from the redox potentials of tyrosine (0.930 V)[49] and the bis-allylic hydrogen of 1,4-pentadiene (0.60 V).[50]

The barrier for the attack of O_2 on the pentadienyl radical is corrected for the solvation energy of O_2 in the enzyme, which lowers the barrier by 2.5 kcal/mol from 11.1 to 8.6 kcal/mol. The exergonicity of the reaction is corrected both for the solvation energy of O_2 and to gas-phase experiments for the reaction enthalpy, increasing the exergonicity by 2.5 and 3.9 kcal/mol, respectively. The reaction energy of this step thus goes from endergonic by 0.8 kcal/mol to exergonic by 5.6 kcal/mol. The barrier of the backward reaction then becomes 14.2 kcal/mol, which agrees rather well with the experimental barrier of 15.5 kcal/mol for the reverse of the autoxidation of methyl linoleate. The autoxidation of methyl linoleate is also an addition of O_2 to a pentadienyl radical forming a conjugated diene peroxyl radical. The experimental barrier was calculated from the rate constant 27 s^{-1}.[51]

The endoperoxide formation, for which there are no corrections introduced, has a barrier of 11.9 kcal/mol, and it is endergonic by 4.9 kcal/mol relative to the immediately preceding intermediate. The experimental formation of an endoperoxide in cholesteryl arachidonate has an estimated rate constant of 800 s^{-1},[52] which corresponds to a barrier of 13.5 kcal/mol, showing that the calculated barrier is in the right region. It should be noted, though, that the energetics of this reaction step are a bit uncertain because there are no experimental values with which to compare the strength of the new bond. The strength of the C−O bond formed in the previous step was found to be underestimated by 3.9 kcal/mol compared to gas-phase experiments. In a similar way, the formation of the peroxide ring might be too endergonic in the calculations, and a correction for such an error would also lower the barrier for the next step going from the peroxyl radical to the bicyclic compound, see below. In this reaction step, a rather complex chemical transformation takes place. A C−O single bond is formed, and a weaker C═C π-bond is broken, and a localized carbon-centered radical is formed from the peroxyl radical. Furthermore, the five-membered ring that is formed is expected to have a strain energy of about 6 kcal/mol.[40] It is therefore quite difficult to estimate the reliability of the calculated energetics of this reaction step.

The cyclization reaction forming the cyclopentane ring in the bicyclic system is not corrected. It has a barrier of 10.0 kcal/mol, and it is exergonic by 13.6 kcal/mol. However, the barrier relative to the resting state of this step (peroxyl radical) is 14.9 kcal/mol. Going from a localized radical to a delocalized allyl radical and forming a C−C bond while breaking a C═C π-bond are similar to the previous reaction step except that this reaction generates a more stable allyl radical. A conclusion that can be drawn from these results is that the difference in exergonicity of the two reactions steps is mainly due to the stability of the different radicals.

For the O_2 attack on the allyl radical, no transition state was found. The exergonicity of the reaction is corrected for the solvation energy of O_2 in the enzyme by 2.5 kcal/mol and for deviations from experimental gas-phase enthalpies for the bond strength by 3.4 kcal/mol. The correction increases the exergonicity of the addition of O_2 from 7.0 kcal/mol to 12.9 kcal/mol. In the experimental gas-phase reaction between the allyl radical and O_2, the barrier was found to be 7.4 kcal/mol, calculated from the rate constant of the reverse reaction. As discussed above, although no transition state was found for this step, an estimate of the barrier can be obtained from the calculations on the similar reaction between O_2 and the pentadienyl radical in a previous step. Maintaining the enthalpy barrier at zero but incorporating entropy and solvation effects from the pentadienyl radical case gives a barrier of 7 kcal/mol, close to the experimental gas-phase value of 7.4 kcal/mol. However, because solvation effects are expected to lower the barrier compared to the gas phase, 7 kcal/mol should be the maximum barrier for this reaction step. In the reaction between O_2 and the pentadienyl radical, solvation effects lowered the barrier by as much as 6 kcal/mol. On the other hand, adding molecular oxygen to a secondary carbon of AA leads to a larger loss of entropy than addition to the primary carbon in the allyl radical of propene, which should raise the barrier by about 1 kcal/mol for the AA case. It can still be estimated that the barrier for this step is so low that the rate of this reaction step might be controlled by diffusion.

The last reaction step in which the peroxyl radical abstracts the hydroxyl hydrogen of Tyr385 is not corrected. The reaction is almost thermoneutral and has a barrier of 10.5 kcal/mol. When experimental BDEs of phenol (87.0 kcal/mol[32]) and alkyl peroxides (around 87 kcal/mol[53]) are compared, the thermoneutrality is expected. The calculations show that the overall reaction for the catalytic cycle is exergonic by almost 37 kcal/mol, which gives a strong driving force for the synthesis of PGG_2.

Comparisons to Experimental Rates. The rate for the conversion of AA to PGG_2 is $k = 90\ s^{-1}$ estimated from the measured specific activity of 100 nmol of O_2/min/μg of protein and assuming that $^2/_3$ of the enzyme is in the catalytic mode.[54] Using transition-state theory on the rate above gives a rate-limiting barrier of 14.8 kcal/mol for the enzymatic reaction.

For the calculated free-energy surface, Figure 11, the two steps with the highest barriers are both close to the experimental rate. The first step, the hydrogen abstraction, has a corrected barrier of 14.5 kcal/mol, and the transition state leading to the bicyclic system with the allyl radical on C13−C15 from the peroxyl radical as the resting state (not the endoperoxide ring) has a corrected barrier of 14.9 kcal/mol. The difference between these two barriers, 0.4 kcal/mol, is smaller than the uncertainty of the calculations. It can therefore not be concluded from the calculations which of these two steps is the rate-limiting one. For the calculated barriers without corrections, the difference is somewhat larger, the uncorrected barrier for the hydrogen abstraction being 12.3 kcal/mol and the uncorrected barrier for the formation of the bicyclic system being 15.7 kcal/mol, see Figure 5. However, the main conclusion is that the barriers for both of these steps agree quite well with the experimental rate-limiting barrier in the enzyme of 14.8 kcal/mol.

On the basis of kinetic isotope effect experiments, it has been concluded that the abstraction of the *proS*-hydrogen is the rate-limiting step.[11] However, the kinetic isotopic effect was measured as the retention of the tritium-labeled arachidonic acid, and according to the present calculations, the hydrogen abstraction is irreversible (strongly exergonic). Therefore, these measurements only give information about the first step, and they cannot be used to determine which step is the rate-limiting one for the enzyme reaction.[55]

IIId. Competing Reactions. In this section, several reactions competing with the formation of PGG_2 are investigated. When the first oxygen molecule reacts with the pentadienyl radical, it can attack at three different positions, at C11, C13, or C15, because the unpaired electron is delocalized about equally over these three carbons, but only the attack at C11 leads to the PGG_2 product. Furthermore, the peroxyl radical formed after the attack of the first molecule of oxygen can terminate the reaction by abstracting the tyrosine hydroxyl hydrogen atom, which would lead to different hydroperoxyl products (labeled HPETE). At a later stage, when the second O_2 molecule reacts with the allyl radical, attack can occur at either C13 or C15, of which only the attack on C15 leads to the observed PGG_2 product. Finally, the second dioxygen might react with the radical localized at C8 after the endoperoxide ring formation and before the formation of the cyclopentane ring, a reaction that does not lead to the PGG_2 product. All of these reactions would lead to different byproducts, of which only two, 11- and 15-HPETE, have been experimentally shown to be formed. Therefore, the other byproducts must be thermodynamically or kinetically unfavorable. This could be due to intrinsic chemical reasons but could also be due to steric effects from the surrounding enzyme, which are not included in the present model. The different competing reaction steps have been investigated, and the calculated free reaction energies and free-energy barriers are discussed below. The values have been corrected according to experimental information in the same way as those for the main reaction path, and the energies below should therefore be comparable to those summarized in Figure 11.

O_2 Attack on the Pentadienyl Radical. As described above, a binding pocket for molecular oxygen created by the enzyme below C11 is the most common explanation for the regio- and enantioselectivity for the reaction of O_2 with the pentadienyl radical. Another possibility is that an uneven spin distribution due to a nonplanar pentadienyl radical with some allyl radical character on C11−C13 gives the selective O_2 attack on C11.[19] In the models used in the calculations, no O_2 binding pocket is included, and neither are the residues in the active site, which might through steric effects give rise to a nonplanar pentadienyl radical. Those proposals can therefore not be investigated within the present model. Instead, the intrinsic energetics for O_2 attack on all three carbons, C11, C13, and C15, of the pentadienyl radical have been investigated, and the results are summarized in Figure 12. The peroxyl radicals obtained from O_2 attack on the two end carbons of the pentadienyl radical, C11 and C15, have almost identical stabilities, with the C11 peroxyl radical only 0.3 kcal/mol lower in energy than the C15 one. On the other hand, the formation of the peroxyl radical on the central carbon, C13 is 5.7 kcal/mol less-stable, which is not surprising

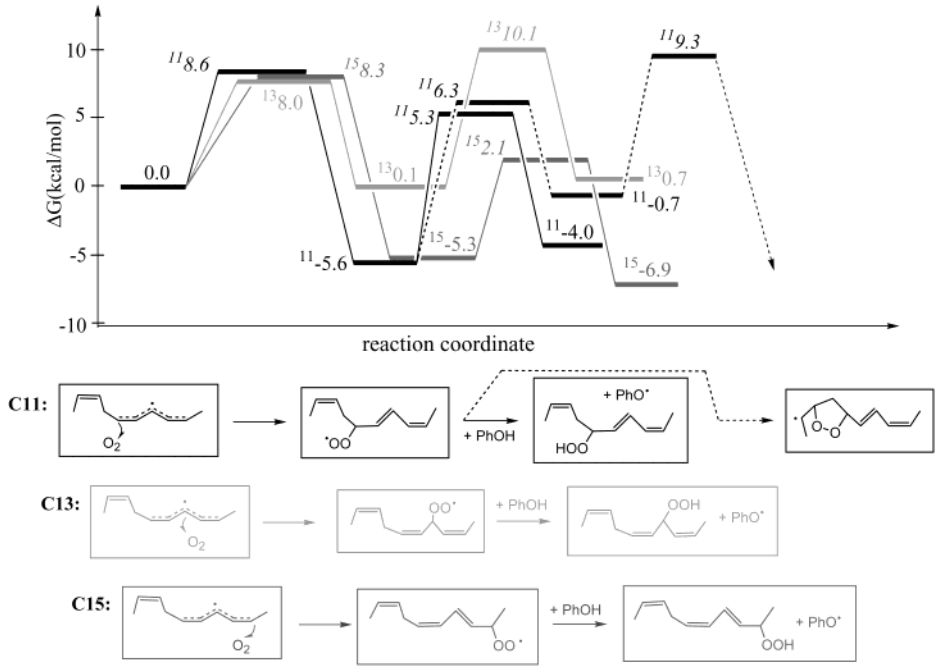

Figure 12. Free-energy surfaces for some competing reactions in the synthesis of PGG_2.

because this isomer does not have conjugated double bonds. The barriers for all three reactions are almost the same, within 0.6 kcal/mol (C11, 8.6; C13, 8.0; C15, 8.3) (Figure 12). As described above the experimental barrier of the backward reaction for addition of dioxygen forming the *conjugated* diene peroxyl radicals of methyl linoleate is 15.5 kcal/mol,[51] which agrees rather well with the calculated barriers of 14.2 (C11) and 13.6 (C15) kcal/mol. The corresponding addition of dioxygen to C13 has a calculated barrier for the backward reaction of 7.9 kcal/mol. This barrier agrees well with the experimental barrier of 8.9 kcal/mol for the reverse reaction of the autoxidation of methyl linoleate forming the *nonconjugated* diene peroxyl radical. The experimental barrier was calculated from the rate constant 1.9×10^6 s^{-1}.[56] The small differences in the barriers for the addition of O_2 show that without constraints caused by the surrounding enzyme, dioxygen would attack all three carbons with very similar rates. O_2 reacting with C13 gives a less-stable product, and because this reaction is reversible (low barrier for the reverse reaction, see also ref 57), the more stable peroxyl radicals on C11 and C15 should be the major products of this step.

HPETE Formation. The peroxyl radical formed after the attack of the first O_2 molecule can abstract a hydrogen atom from Tyr385, which leads to HPETE byproducts. Only 11- and 15-HPETE have been identified experimentally,[39] which is in agreement with the results from the previous paragraph showing that peroxyl radical formation on C11 or C15 is more favorable than that on C13. The hydrogen abstraction reaction has been investigated for all three possible peroxyl radicals, C11, C13, and C15, and the results are here compared to each other and to the main reaction in which the C11 peroxyl radical forms the endoperoxide ring, see Figure 12. The abstraction reactions have rather low barriers for both the C11 and the C15 peroxyl, 10.9 and 7.4 kcal/mol, respectively. The reaction of the C15 peroxyl radical is found to be exergonic by 1.6 kcal/mol, making the 15-HPETE product the most-stable structure on the free-energy surface, see Figure 12. The hydrogen abstraction by the 11-peroxyl is slightly endothermic, by 1.6 kcal/mol, making 11-HPETE + Tyr385$^\bullet$ less stable than 15-HPETE + Tyr385$^\bullet$, as well as the 11-peroxyl radical + Tyr385. The energetic differences between C11 and C15 peroxyls come mainly from entropy and solvent effects, the enthalpies are very similar. On the other hand, for the C11 peroxyl radical, the hydrogen abstraction reaction is more favorable than the endoperoxide ring formation leading to the PGG_2 product. Starting at the C11 peroxyl radical, the endoperoxide ring formation has a barrier that is 1.0 kcal/mol higher and the endoperoxide product is 3.3 kcal/mol less stable than the 11-HPETE product, see Figure 12. One should keep in mind though, that the C−O bond strength in the endoperoxide ring is a bit insecure, see above in the section on corrected free-energy surface. Finally, the hydrogen abstraction by the C13 peroxyl radical has a barrier of 10.0 kcal/mol and is endergonic by 0.6 kcal/mol, making the 13-HPETE product the least stable one, 0.7 kcal/mol above the initial pentadienyl radical and free O_2. These results are summarized in Figure 12, in which the main reaction path also is shown (dashed curve). From this figure, it is clear that 13-HPETE formation following an attack on C13 is unfavorable and will not occur, in agreement with experimental observations. However, the results also show that within the present model O_2 attack on C11 and C15 and the following hydrogen abstractions by these peroxyl radicals are energetically more favorable than the main reaction path leading to PGG_2 formation. The hydrogen abstraction by the nonconjugated diene peroxyl radical of methyl linoleate from the substituted phenol α-tocopherol (vitamin E) has a barrier of 8.5 kcal/mol. This barrier was calculated from the rate constant 3.8×10^6 s^{-1} [56] and agrees satisfactorily with the calculated barrier of 10.0 kcal/mol for the corresponding reaction between the C13 peroxyl radical and Tyr385.

To understand the fact that the PGG_2 is the main product of the native enzyme, about 95%, with only 3% corresponding to 11*R*-HPETE and 2% to 15*S*- or 15*R*-HPETE formation,[39] it must be remembered that while 11- and 15-HPETE are the final products in these reaction paths, the endoperoxide radical at C8 will react further in a quite exergonic reaction (dashed curve in Figure 12). The calculated potential curves show that the reaction of molecular oxygen with the pentadienyl radical and the following hydrogen abstraction from Tyr385 are reversible reactions, which can return to the main reaction path. The most stable HPETE product, 15-HPETE, faces a total barrier of

15.2 kcal/mol to regenerate the pentadienyl radical, and 11-HPETE faces a barrier of only 9.3 kcal/mol to return to the 11-peroxyl radical. This means that if AA remains sufficiently long in the active-site pocket the exergonicity of the reactions following endoperoxide ring formation would push the reaction toward the formation of the PGG_2 product. The uncertainty in the calculations allows the possibility that the reversible reactions are faster than the overall rate of the reaction leading to PGG_2 because the difference is only 0.3 kcal/mol. The difference in energetic cost for 11- and 15-HPETE to dissociate from the enzyme and the backward reaction to reenter the catalytic manifold would then give the ratio of 15-HPETE, 11-HPETE, and PGG_2. The exergonicity of 27 kcal/mol for the formation of PGG_2 from the endoperoxide ring intermediate will push the equilibrium toward PGG_2 if dissociation of 11- and 15-HPETE is slow.

It should be pointed out that the structure of the native enzyme is not expected to be optimal for the hydrogen abstraction from Tyr385 by the 11- or 15-peroxyl radicals. The hydrogen abstraction from Tyr385 occurring in the PGG_2 production from a C15 peroxyl radical occurs first in the last reaction step after the ω-end of the substrate has been pulled into the active-site pocket. In the calculations described above for the formation of 11- and 15-HPETE, there are no constraints introduced and the Tyr385 can adopt an optimal position for the hydrogen atom abstractions, but geometric constraints in the enzyme will probably keep the peroxyl radicals away from Tyr385. To overcome such steric hindrance costs energy, which will raise the energy of the 11-HPETE and 15-HPETE products and also the barriers for the hydrogen abstraction from Tyr385 by the C11 and C15 peroxyl radicals. The increase in energy corresponds to the energy needed to change the conformation of the substrate to a reactive one in the active site of PGHS. The higher energy of the HPETE products will increase the rate of the reverse reactions, and the increased barriers for the hydrogen abstraction will decrease the rate of the forward side reactions. Both effects thus change the ratio between the HPETE and PGG_2 products in favor of PGG_2 formation.

It is finally interesting to note that the experimental investigation leading to a distribution among the different products, PGG_2, 11*R*-, 15*R*- and 15*S*-HPETE, indicates that the AA substrate can assume at least three catalytically productive conformations within the cyclooxygenase site of PGHS-1 and that each of the observed products corresponds to one of these conformations.[39] These results indicate that the ratio between the products is affected also by differences in the stabilities of the enzyme−substrate complexes.

O_2 Attack on the Allyl Radical. The delocalized nature of the allyl radical formed after the cyclopentane ring closure implies the possibility for the second dioxygen to attack either C13 or C15, which after hydrogen atom abstraction from Tyr385 would lead to two different peroxides. Only the C15 peroxide is observed experimentally as the final PGG_2 product. The most common explanation is again O_2 binding to a pocket well-positioned for attacking at C15 after the two cyclization steps. Comparing the energies of the two reactions shows that the peroxyl radical on C15 is more stable than the one on C13 by only 1.7 kcal/mol. Because the energetics of the final hydrogen abstraction is the same for the two peroxyl radicals, in contrast to the experimental observation, almost 10% of the C13 peroxyl radical should be formed, assuming thermodynamical equilibrium. Another factor could be that the peroxyl radical on C13 is less favorably positioned for the final step of abstracting the hydrogen back from Tyr385 as discussed in the pentadienyl case above. This could mean that the formation of C13 peroxide is so slow that, assuming thermodynamical equilibrium, only the C15 peroxide is formed. Another possibility is that the C13 position is blocked for dioxygen attack by some nearby residues in the active site. Because the peroxide group on C13 is never seen, there must in reality be a larger advantage for O_2 to attack only C15 than can be described within the models used in the present study.

O_2 Attack on the C8 Radical of the Endoperoxide Intermediate. Instead of the reaction between the C8 radical and C12 forming the bicyclic system with a cyclopentane ring, a second molecule of oxygen might attack the C8 radical. The formation of such a C8-based peroxyl radical, which does not occur in the enzyme according to experimental information, has been investigated, and it turns out that such a reaction is exergonic by as much as 19 kcal/mol and it has no enthalpy barrier. Like for the previously discussed reactions with molecular oxygen, though, there is a large entropy effect on this reaction step, which leads to a free-energy barrier, probably less than 7 kcal/mol (see the discussion in section IIIa on the addition of O_2 to the allyl radical). Thus the calculations indicate that the barrier for the C8-peroxyl formation is lower than the barrier of 10.0 kcal/mol obtained for formation of the cyclopentane ring in the main reaction path, and why a C8-peroxyl is not formed cannot be explained. It should also be noted that because of the large exergonicity for the O_2 addition, such a reaction step would not be reversible. It is therefore concluded that the O_2 addition at this point is avoided by steric effects of the protein, which cannot be described within the present model.

IV. Conclusions

The formation of prostaglandin G_2, occurring in the cyclooxygenase site of prostaglandin H synthase, has been investigated. A free-energy surface for the mechanism suggested by Hamberg and Samuelsson[11] was computed using the B3LYP hybrid density functional. The suggested mechanism, starting from an active-site tyrosyl radical and the arachidonic acid substrate, consists of six separate steps. Intermediates and transition states have been located for each individual reaction. Two of the steps involve addition of molecular oxygen, and in these cases, the enthalpy barrier was found to be very low or nonexistent, but the large entropy loss leads to free-energy barriers for these reactions. For several steps, comparisons can be made with similar chemical reactions studied experimentally, and in these cases, corrections were introduced to account for the minor inaccuracy of the B3LYP values. The resulting free-energy curve is presented in Figure 11, and from this, it can be concluded that the overall reaction has a large driving force, computed to be 37 kcal/mol. Concerning the rate-limiting step, it is found that two steps have almost the same activation energy, step 1 corresponding to the hydrogen atom abstraction by the tyrosyl radical (barrier of 14.5 kcal/mol) and step 4 corresponding to the cyclopentane ring formation (barrier of 14.9 kcal/mol relative to its peroxyl radical resting state). Both of these values are very close to the experimentally determined activation energy of 14.8 kcal/mol, and the difference between the two calculated barriers is smaller than the B3LYP uncertainty. Therefore, from the calculations, it is impossible to determine which of these two steps is rate-limiting.

Several competing reaction steps not leading to the main prostaglandin G_2 product have also been investigated. The competing reactions are mainly concerned with when and where molecular oxygen attacks the substrate radical at different steps of the reaction path. Two minor byproducts have been observed

experimentally, 11-HPETE and 15-HPETE, and the calculated energetics are in agreement with the formation of these products. However, the calculated energetics can explain neither why certain other possible byproducts are not formed, nor the observed distribution among the products actually formed. It is therefore concluded that steric effects from the surrounding protein, not included in the model used in the calculations, determine the selectivity between these different reaction paths.

References and Notes

(1) Herschman, H. R. *Biochim. Biophys. Acta* **1996**, *1299*, 125−140.

(2) Picot, D.; Loll, P. J.; Garavito, R. M. *Nature* **1994**, *367*, 243−249.

(3) Luong, C.; Miller, A.; Barnett, J.; Chow, J.; Ramesha, C.; Browner, M. F. *Nat. Struct. Biol.* **1996**, *3*, 927−933.

(4) Kurumbail, R. G.; Stevens, A. M.; Gierse, J. K.; McDonald, J. J.; Stegeman, R. A.; Pak, J. Y.; Gildehaus, D.; Miyashiro, J. M.; Penning, T. D.; Seibert, K.; Isakson, P. C.; Stallings W. C. *Nature* **1996**, *384*, 644−648.

(5) Malkowski M. G.; Ginell, S. L.; Smith, W. L.; Garavito, R. M. *Science* **2000**, *289*, 1933−1937.

(6) Smith, W. L.; Eling, T. E.; Kulmacz, R. J.; Marnett, L. J.; Tsai A.-L. *Biochemistry* **1992**, *31*, 3−7.

(7) Kulmacz, R. J.; Tsai, A.-L.; Palmer G. *J. Biol. Chem.* **1987**, *262*, 10524−10531.

(8) Karthein, R.; Dietz, R.; Natsainczyk, W.; Ruf, H. H. *Eur. J. Biochem.* **1988**, *171*, 313−320.

(9) Hsi, L. C.; Hoganson, C. W.; Babcock, G. T.; Smith, W. L. *Biochem. Biophys. Res. Commun.* **1994**, *202*, 1592−1598.

(10) Xiao, G.; Tsai, A.-L.; Palmer, G.; Boyar, W. C.; Marshall, P. J.; Kulmacz, R. J. *Biochemistry* **1997**, *36*, 1836−1845.

(11) Hamberg, M.; Samuelsson, B. *J. Biol. Chem.* **1967**, *242*, 5336−5343.

(12) Schneider, C.; Boeglin, W. E.; Prusakiewicz, J. J.; Rowlinson, S. W.; Marnett, L. J.; Samel, N.; Brash, A. R. *J. Biol. Chem.* **2002**, *277*, 478−485.

(13) Thuresson, E. D.; Lakkides, K. M.; Rieke, C. J.; Sun, Y.; Wingerd, B. A.; Micielli, R.; Mulichak, A. M.; Malkowski, M. G.; Garavito, R. M.; Smith, W. L. *J. Biol. Chem.* **2001**, *276*, 10347−10359.

(14) Thuresson, E. D.; Malkowski, M. G.; Lakkides, K. M.; Rieke, C. J.; Mulichak, A. M.; Ginell, S. L.; Garavito, R. M.; Smith, W. L. *J. Biol. Chem.* **2001**, *276*, 10358−10365.

(15) Malkowski, M. G.; Thuresson, E. D.; Lakkides, K. M.; Rieke, C. J.; Micielli, R.; Smith, W. L.; Garavito, R. M. *J. Biol. Chem.* **2001**, *276*, 37547−37555.

(16) Tsai, A.-L.; Kulmacz, R. J.; Palmer G. *J. Biol. Chem.* **1995**, *270*, 10503−10508.

(17) Tsai, A.-L.; Palmer, G.; Xiao, G.; Swinney, D. C.; Kulmacz, R. J. *J. Biol. Chem.* **1998**, *273*, 3888−3894.

(18) Peng, S.; Okeley, N. M.; Tsai, A.-L.; Wu, G.; Kulmacz, R. J.; van der Donk, W. A. *J. Am. Chem. Soc.* **2001**, *123*, 3609−3610.

(19) Peng, S.; Okeley, N.; Tsai, A.-L.; Wu, G.; Kulmacz, R. J.; van der Donk, W. A. *J. Am. Chem. Soc.* **2002**, *124*, 10785−10796.

(20) Becke, A. D. *J. Chem. Phys.* **1993**, *98*, 5648−5652.

(21) Lee, C.; Yang, W.; Parr, R. G. *Phys. Rev. B* **1988**, *37*, 785−789.

(22) Tannor, D. J.; Marten, B.; Murphy, R.; Friesner, R. A.; Sitkoff, D.; Nicholls, A.; Ringnalda, M.; Goddard, W. A., III; Honig B. *J. Am. Chem. Soc.* **1994**, *116*, 11875−11882.

(23) Blomberg, M. R. A.; Siegbahn, P. E. M.; Babcock, G. T. *J. Am. Chem. Soc.* **1998**, *120*, 8812−8824.

(24) Siegbahn, P. E. M.; Blomberg, M. R. A. *Annu. Rev. Phys. Chem.* **1999**, *50*, 221−249.

(25) Siegbahn, P. E. M.; Blomberg, M. R. A. *Chem. Rev.* **2000**, *100*, 421−437.

(26) Blomberg, M. R. A.; Siegbahn, P. E. M. *J. Phys. Chem. B* **2001**, *105*, 9375−9386.

(27) Dapprich, S.; Komáromi, I.; Byun, K. S.; Morokuma, K.; Frisch, M. J. *J. Mol. Struct. (THEOCHEM)* **1999**, *462*, 1−21.

(28) Svensson, M.; Humbel, S.; Froese, R. D. J.; Matsubara, T.; Sieber, S.; Morokuma, K. *J. Phys. Chem.* **1996**, *100*, 19357−19363.

(29) Humbel, S.; Sieber, S.; Morokuma, K. *J. Chem. Phys.* **1996**, *105*, 1959−1967.

(30) Frisch, M. J.; Trucks, G. W.; Schlegel, H. B.; Scuseria, G. E.; Robb, M. A.; Cheeseman, J. R.; Zakrzewski, V. G.; Montgomery, J. A., Jr.; Stratmann, R. E.; Burant, J. C.; Dapprich, S.; Millam, J. M.; Daniels, A. D.; Kudin, K. N.; Strain, M. C.; Farkas, O.; Tomasi, J.; Barone, V.; Cossi, M.; Cammi, R.; Mennucci, B.; Pomelli, C.; Adamo, C.; Clifford, S.; Ochterski, J.; Petersson, G. A.; Ayala, P. Y.; Cui, Q.; Morokuma, K.; Malick, D. K.; Rabuck, A. D.; Raghavachari, K.; Foresman, J. B.; Cioslowski, J.; Ortiz, J. V.; Stefanov, B. B.; Liu, G.; Liashenko, A.; Piskorz, P.; Komaromi, I.; Gomperts, R.; Martin, R. L.; Fox, D. J.; Keith, T.; Al-Laham, M. A.; Peng, C. Y.; Nanayakkara, A.; Gonzalez, C.; Challacombe, M.; Gill, P. M. W.; Johnson, B. G.; Chen, W.; Wong, M. W.; Andres, J. L.; Head-Gordon, M.; Replogle, E. S.; Pople, J. A. *Gaussian 98*, revision A.11.3; Gaussian, Inc.: Pittsburgh, PA, 1998.

(31) Dewar, M. J. S.; Zoebisch, E. G.; Healy, E. F.; Stewart, J. J. P. *J. Am. Chem. Soc.* **1985**, *107*, 3902−3909.

(32) Laarhoven L. J. J.; Mulder, P.; Wayner, D. D. M. *Acc. Chem. Res.* **1999**, *32*, 342−349.

(33) Trenwith A. B. *J. Chem. Soc., Faraday Trans. 1* **1982**, *78*, 3131−3136.

(34) Froese, R. D. J.; Humbel, S.; Svensson, M.; Morokuma, K. *J. Phys. Chem. A* **1997**, *101*, 227−233.

(35) Curtiss, L. A.; Raghavachari, K.; Pople, J. A. *J. Chem. Phys.* **1993**, *98*, 1293−1298.

(36) *Jaguar 4.1* Schrodinger, Inc.: Portland, OR, 2000.

(37) Bhattacharyya, D. K.; Lecomte, M.; Rieke, C. J.; Garavito, R. M.; Smith, W. L. *J. Biol. Chem.* **1996**, *271*, 2179−2184.

(38) Tsai, A.-L.; Kulmacz, R. J.; Palmer, G. *J. Biol. Chem.* **1995**, *270*, 10503−10508.

(39) Thuresson, E. D.; Lakkides, K. M.; Smith, W. L. *J. Biol. Chem.* **2000**, *275*, 8501−8507.

(40) Streitweiser, A.; Heathcook, C. H.; Kosower, E. M. *Introduction to Organic Chemistry*, 4th ed.; Macmillan Publishing Company: New York, 1992.

(41) Fischer, K.; Noll, O.; Gmehling, J. *J. Chem. Eng. Data* **2001**, *46*, 1504−1505.

(42) Fischer, K.; Wilken M. *J. Chem. Thermodyn.* **2001**, *33*, 1285−1308.

(43) Hesse, P. J.; Battino, R.; Scharlin, P.; Wilhelm, E. *J. Chem. Eng. Data* **1996**, *41*, 195−201.

(44) Hesse, P. J.; Battino, R.; Scharlin, P.; Wilhelm, E. *J. Chem. Thermodyn.* **1999**, *31*, 1175−1181.

(45) Rettich, T. R.; Battino, R.; Wilhelm, E. *J. Chem. Thermodyn.* **2000**, *32*, 1145−1156.

(46) Wirstam, M.; Lippard, S. J.; Friesner, R. A. Personal communication, 2002.

(47) Zils, R.; Inomata, S.; Imamura, T.; Miyoshi, A.; Washida, N. *J. Phys. Chem. A* **2001**, *105*, 1277−1282.

(48) Ruiz, R. P.; Bayes, K. D.; Macpherson, M. T.; Pilling, M. J. *J. Phys. Chem.* **1981**, *85*, 1622−1624.

(49) Harriman, A. *J. Phys. Chem.* **1987**, *91*, 6102−6104.

(50) Koppenol, W. H. *FEBS Lett.* **1990**, *264*, 165−167.

(51) Porter, N. A.; Wujek, D. G. *J. Am. Chem. Soc.* **1984**, *106*, 2626−2629.

(52) Yin, H.; Havrilla, C. M.; Morrow, J. D.; Porter, N. A. *J. Am. Chem. Soc.* **2002**, *124*, 7745−7754.

(53) Jonsson, M. *J. Phys. Chem.* **1996**, *100*, 6814−6818.

(54) Kulmacz, R. J.; Pendelton, R. B.; Lands, W. E. M. *J. Biol. Chem.* **1994**, *269*, 5527−5536.

(55) Northrop, D. B. *Biochemistry* **1981**, *20*, 4056−4061.

(56) Tallman, K. A.; Pratt, D. A.; Porter, N. A. *J. Am. Chem. Soc.* **2001**, *123*, 11827−11828.

(57) Chan, H. W.-S.; Levett, G.; Matthew, J. A. *J. Chem. Soc., Chem. Commun.* **1978**, 756−757.